A Room-Temperature Ionic-Liquid-Templated Proton-Conducting Gelatinous Electrolyte

Zhiying Li,[†] Hongtao Liu,[†] Yang Liu,[†] Ping He,[†] and Jinghong Li[†,‡,*]

State Key Laboratory of Electroanalytical Chemistry, Changchun Institute of Applied Chemistry, Chinese Academy of Sciences, Changchun 130022, China, and Department of Chemistry, Tsinghua University, Beijing 100084, China

Received: June 24, 2004; In Final Form: September 1, 2004

Novel proton-conducting gelatinous electrolytes templated by room-temperature ionic liquid (RTIL) 1-butyl-3-methyl-imidazolium-tetrafluoroborate ($BMImBF_4$) have been prepared in methylsisesquioxane backbone containing H_3PO_4, and the influences of the RTIL on the structure, morphology, thermal stability, and electrochemical properties of the gelatinous electrolytes have been examined. X-ray diffraction and scanning electron microscopy proved that $BMImBF_4$ acted as structure-directing template during the sol−gel process of methyl-trimethoxysilane. X-ray photoelectron spectra and infrared spectroscopy demonstrated that the hydrogen-bonding was formed between $BMImBF_4$ and H_3PO_4. The electrolytes had good thermal stability up to 300 °C and showed superior mechanical and electrochemical properties. A room-temperature conductivity of 1.2×10^{-3} S cm^{-1} was obtained for the electrolyte at the molar ratio of RTIL/Si/H_3PO_4 0.3/1/1, and its electrochemical window was up to 1.5 V. The satisfactory thermomechanical and electrochemical properties of the obtained electrolytes make them promising materials in various electrochemical devices, such as batteries, fuel cells, sensors, and electrochromic windows.

1. Introduction

Proton-conducting electrolytes are emerging as useful materials because of the possibility of their application in various electrochemical devices such as high energy batteries, fuel cells, humidity and gas sensors, and electrochromic windows that work from subambient to moderate temperature.[1] To date, most of the proton-conducting systems studied are based either on the inorganic acids and their salts or on the polymer complexes and alkoxides hydrogels with strong inorganic acids.[1,2] Inorganic acids (such as H_2SO_4, H_3PO_4 or heteropolyacids) have excellent electrical properties, but their high chemical activity is a serious drawback for practical applications.[3,4] Polymer electrolytes doped with proton donors have recently attracted much attention because of their high proton-conducting, chemical and electrochemical stability, and good processability of polymer matrixes.[5−7] Conventional perfluorosulfonic polymer Nafion membranes have also been used in fuel cells, but they normally need humidifying under almost saturated water vapor at the operation temperature and they tend to degrade at temperature over 100 °C.[8,9] Hydrogel systems doped with several proton-conducting materials such as H_3PO_4 and its salts, NH_4BF_4 or NH_4SCN, were described in detail by Chandra et al.[10−12] and Matsuda et al.[13−15] Phosphosilicate gels prepared from alkoxysilane and H_3PO_4 by the sol−gel method could show high proton conductivities even in the medium-temperature range with low humidity. However, on storage, the entrapped electrolyte solution leached out or resulted in the whisker growth of the dopant salt. Furthermore, the prepared gel powder needs to be pressed into a pellet or rod before usage, and the doped liquid material can be seen oozing out during pressing or cutting the gel ingots.[10] Thus, further work needs to be done to improve the physical and chemical properties of the proton-conducting electrolytes.

Room-temperature ionic liquids (RTILs) are organic salts with low melting points, sometimes as low as −96 °C,[16] and have a stable liquid range of over 300 K. Typical RTILs have unusual properties including nonvolatility, nonflammability, wide electrochemical windows, higher ionic conductivity, and excellent thermal and chemical stability. RTILs have been widely used as "green" organic solvents[17] and as electrolytes in batteries,[18,19] fuel cells,[20,21] double-layer capacitors,[22−24] dye-sensitive solar cells,[25−27] and actuators.[28] Recently, Antonietti et al.[29−32] have reported a few studies on the preparation of novel monolithic super-microporous lamellar silica with RTIL as the template employed with the nanocasting technique. However, no silica gel doped with RTIL along with protonic acid as ambient temperature proton electrolyte has been addressed yet to our knowledge.

In the present work, we used methyl-trimethoxysilane as the sol−gel precursor, 1-butyl-3-methyl-imidazolium-tetrafluoroborate as the template to produce RTIL-methylsisesquioxane electrolyte, and H_3PO_4 as the proton donor entrapped in the methylsisesquioxane (MSQ) matrix. The main goal was to combine the good chemical and electrochemical stability of RTIL with the high proton conductivity and mechanical properties of silica gel to develop novel RTIL-templated proton-conducting composite materials that are suitable for use in electrochemical devices. Because of the entrapment of RTIL, the electrolytes show superior thermal and mechanical properties to the glassy silica, and the electrochemical window reaches 1.5 V and the room-temperature conductivity can be up to 1.2×10^{-3} S cm^{-1}.

2. Experimental Section

2.1. Chemicals. 1-Butyl-3-methyl-imidazolium-tetrafluoroborate ($BMImBF_4$, ≥98%) and methyl-trimethoxysilane (MT-

* Corresponding author. Tel. and fax: +86-431-5262243; e-mail: jhli@mail.tsinghua.edu.cn.
‡ Tsinghua University.
† Chinese Academy of Sciences.

10.1021/jp047252x CCC: $27.50
Published on Web 10/16/2004

SCHEME 1: Schematic Representation of Steps Involved in the RTIL-Templated Proton-Conducting Electrolyte Preparation

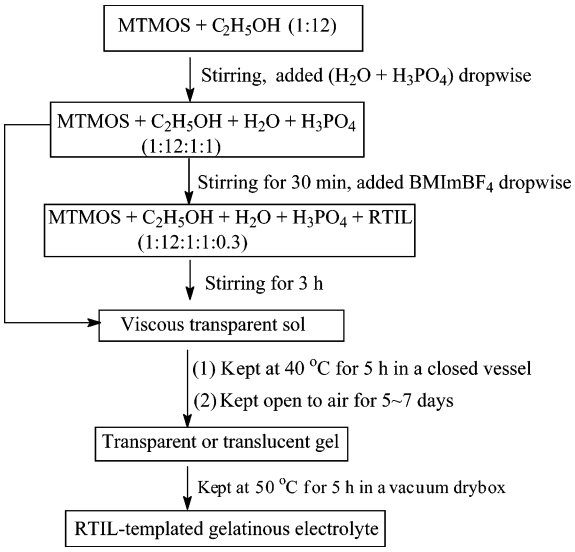

MOS) were purchased from Solvent Innovation and Sigma, respectively. H_3PO_4 (85%) and ethanol were purchased from Beijing Chemicals Company. Water was purified with Milli-Q (18.3 MΩ) water system.

2.2. Preparation of RTIL-Templated Proton-Conducting Gelatinous Electrolyte. The sol−gel method was adopted here to prepare RTIL-templated proton-conducting gelatinous electrolyte (presented as IL-GE). MTMOS was used as starting material, H_2O and H_3PO_4 and $BMImBF_4$ with desired ratio were added dropwise to control the rate of gelation (see Scheme 1). EtOH diluted MTMOS was gradually hydrolyzed by adding the diluted H_3PO_4 aqueous solution dropwise under stirring. After reaction for 30 min, $BMImBF_4$ was added to the hydrolyzed solution. Keeping continual stirring for 3 h, a homogeneous solution phase was formed. The molar ratio of MTMOS/EtOH/H_2O/H_3PO_4/RTIL of the resultant phase was 1/12/1/1/0.3 (labeled as IL-GE). The sol was then kept in a closed vessel at 40 °C for 5 h to form wet MSQ gel and then kept open to air at room temperature for a week. The final softish translucent gel was dried at 50 °C in a vacuum for 5 h to remove the alcohol and the formed methanol in the gel before further characterization. The gelatinous electrolyte in the absence of RTIL (presented as GE) was prepared with the same procedures used for comparison purpose.

2.3. Characterization. The X-ray diffraction (XRD) pattern was recorded with a RIGAKU D/max-II B X-ray diffractometer using a Cu-K_α radiation (1.5406 Å) of 40 kV and 20 mA.

Fourier transform infrared spectroscopy (FT-IR) was conducted at FTS135 infrared spectroscopy (Bio-Rad, U.S.). FT-IR transmission spectra of the gelatinous electrolytes were obtained by forming thin transparent KBr pellet containing the interesting materials.

Scanning electron microscopy (SEM) was performed on JEOL-JXA-840 (JEOL, Japan) electron microscopy operating at 20 kV. To take the SEM micrograph, the prepared electrolyte was calcinated at 500 °C for 5 h, and the final product was ground into a powder for further characterization.

X-ray photoelectron spectra (XPS) was conducted using a VG ESCALAB MK II spectrometer (VG Scientific, U.K.) employing a monochromatic Mg-K_α X-ray source ($h\nu = 1253.6$ eV). Peak position was internally referenced to the C_{1s} peak at 284.6 eV. The electrolyte was pretreated at 200 °C for 5 h before characterization.

The thermal gravimetry analysis (TGA) and differential thermal analysis (DTA) were carried out using a Perkin-Elmer thermal analysis TG/DTA system. Measurements were made heating from 20 to 700 °C, at a heating rate of 10 °C/min under N_2 atmosphere.

The dynamic elastic modulus and dissipation (tan δ) of the gelatinous materials were measured by Metravib MAK-04 Viscoanalyzer (France) at 10 Hz in the temperature range from −150 to 150 °C at a heating rate of 3 °C/min under N_2 atmosphere. For the gelatinous electrolytes prepared in this work, a sample holder for measuring in shear mode was the most suitable technique.

Electrochemical window of the electrolyte was checked by cyclic voltammetry using a three-electrode configuration. Both working electrode and counter electrode were stainless steels (SS), and a Ag wire was used as pseudo-reference electrode. The cyclic voltammetry was performed at room temperature by using a CHI 832 electrochemical station (CHI Inc., U.S.).

The ionic conductivity of the electrolyte was evaluated using a complex impedance method in the temperature range of 17−70 °C. The sample was sandwiched between two stainless steel blocking electrodes with a PTFE spacer with a circular hole (1 mm thick, 0.5 cm^2) for holding the gel electrolyte and was placed in a temperature-controlled furnace. The impedance measurements were carried out on a Solartron 1255B Frequency Response Analyzer and a Solartron 1470 Battery Test Unit (Solartron Inc., U.K.) coupled with a computer. The impedance spectra were recorded with the help of ZPlot/ZView software (Scribner Associates Inc.) under an ac perturbation signal of 10 mV over the frequency range of 100 kHz to 1 Hz. The relative humidity was about 25% during the experiment.

3. Results and Discussion

In this work, a translucent gelatinous IL-GE was obtained. Unlike the conventional silica, the IL-GE did not shrink with time and showed no obvious change during storage. The GE obtained was a transparent MSQ ($CH_3SiO_{1.5}$) monolith, but the gel in the wet state was likely to shrink with time and became hard and crisp. The GE monolith was pressed into pellet to use as electrolyte, and H_3PO_4 could be seen oozing out from the ingot during pressing or storage. The presence of RTIL prolonged the gelation time in comparison to the GE system. The reason for this could be that a certain amount of $BMImBF_4$ was incorporated on the surface of the MSQ cluster, and the growth of the cluster was slowed or stopped. Further evidences for the difference of IL-GE and GE are shown in the following XRD, SEM, XPS, and so forth.

3.1. X-ray Diffraction. The X-ray diffractograms of the as-prepared and calcinated GE and IL-GE are shown in Figure 1. For the as-prepared samples, two broad bands were observed similarly, indicating amorphous matrix for both GE and IL-GE. There was no visible difference between the XRD patterns of the as-prepared GE and IL-GE. However, their XRD patterns changed after the samples were heat-treated at 300 °C for 1 h. The process of heat treatment made the materials crystallized and ordered. Two sharp peaks at about 24° and 39° appeared, and the diffractive peaks of the heat-treated IL-GE had a slight right shift compared with that of GE, which might be attributed to different orientation of the MSQ under different circumstances since the RTIL was almost nonvolatile at 300 °C.[33]

Chandra et al.[12] reported that the entrapped H_3PO_4 solution increased the amorphicity and that there was no characteristic

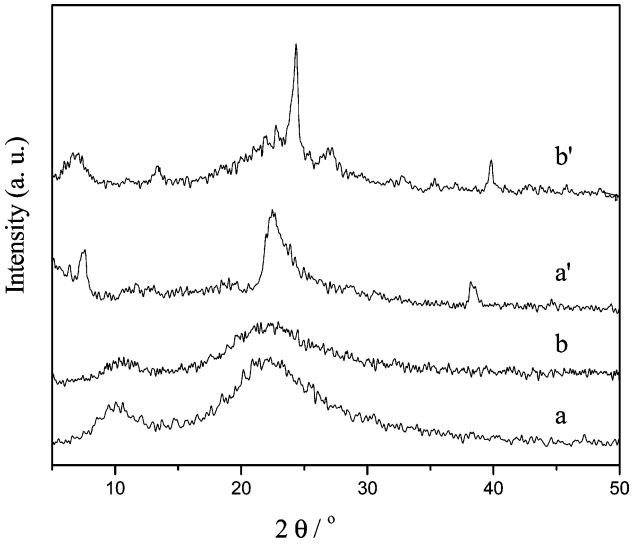

Figure 1. Powder XRD patterns for the electrolytes (a, a′) without and (b, b′) with RTIL. The electrolyte samples were (a, b) as-prepared and (a′, b′) heat-treated at 300 °C for 1 h, respectively.

peak of H_3PO_4 and no new compound formation in the silica matrix. Antonietti et al.[29−32] have reported a few studies on using RTILs as the template during the hydrolysis and polycondensation of silica precursor. Thus, the right shift of the diffractive peaks of the heat-treated IL-GE confirmed that RTIL was used as the structure-directing template during the sol−gel process, creating a different oriented MSQ phase.

3.2. Scanning Electron Microscopy. The SEM images of the porous materials are shown in Figure 2. From the image of IL-GE (Figure 2B), we could see that solid particles connect to each other and form a three-dimensional network. However, the micrograph of GE (Figure 2A) exhibited a much coarser structure consisting of larger smooth plates, and the micropores in GE would be formed in the primary particles. The difference can be ascribed to that the ternary porogen mixture of RTIL-H_3PO_4−H_2O influenced the mechanism of phase separation, nucleation, aggregation, and pore formation. Since RTIL consists entirely of large cations and anions, the electrostatic interactions between the $BMImBF_4$ molecule and the Si−OH species generated in situ influenced the network structure and particle dimension of IL-GE.[34] On the other hand, during the process of calcination, the volatile solvent in the GE was removed quickly, the gel shrank, and the pore might have disappeared. As for the sample of IL-GE, because RTIL was nonvolatile to 300 °C, the porous structure remained.

3.3. X-ray Photoelectron Spectra. Figure 3 shows Si_{2p} and P_{2p} spectra of the GE and IL-GE. We can see that the Si_{2p} peak of 102.8 eV was almost unchanged with the addition of the RTIL, whereas the binding energy of P_{2p} decreased from 134.7 to 133.4 eV. $BMImBF_4$ was likely to form hydrogen-bonding,[29] and the hydrogen-bonding between $BMImBF_4$ and H_3PO_4 or water was formed when it was added into the matrix. The shift of P_{2p} toward the lower binding energy values indicated a decreased ionic nature of the P−O bond, which resulted from the interaction of the hydrogen-bonding. Naturally, the hydrogen-bonding between $BMImBF_4$ and H_3PO_4 or water tethered the proton, which was reflected by a decrease in the ionic conductivity,[35] as shown below.

3.4. Fourier Transform Infrared Spectroscopy. The IR spectra of GE, IL-GE, and neat $BMImBF_4$ are shown in Figure 4. The dominant peaks of GE[36] (curve a) are the H−O−H bending vibration of the adsorbed water at 1636 cm^{-1}, the

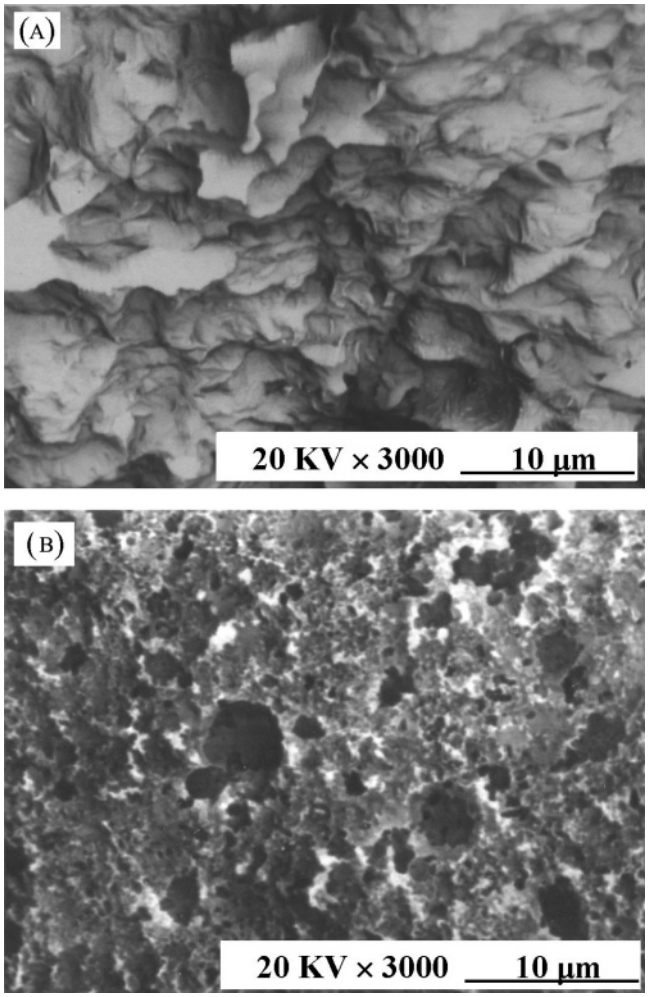

Figure 2. SEM micrographs of the electrolytes (A) without and (B) with RTIL after calcinated at 500 °C for 5 h.

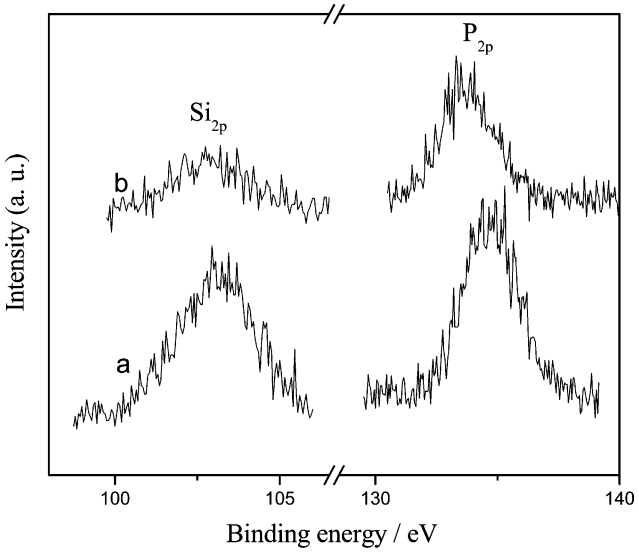

Figure 3. XPS spectra of Si_{2p} and P_{2p} of the electrolytes (a) without and (b) with RTIL.

$Si-CH_3$ symmetric stretch at 1274 cm^{-1}, the siloxane bonds (Si−O−Si) at 1132 and 1027 cm^{-1}, and the $O-Si-CH_3$ vibration at 782 cm^{-1}.

In curve b, a broad band in the range of 900−1200 cm^{-1} was observed. It was due to the overlap of the Si−O−Si asymmetric stretching vibration, the P−O asymmetric stretching

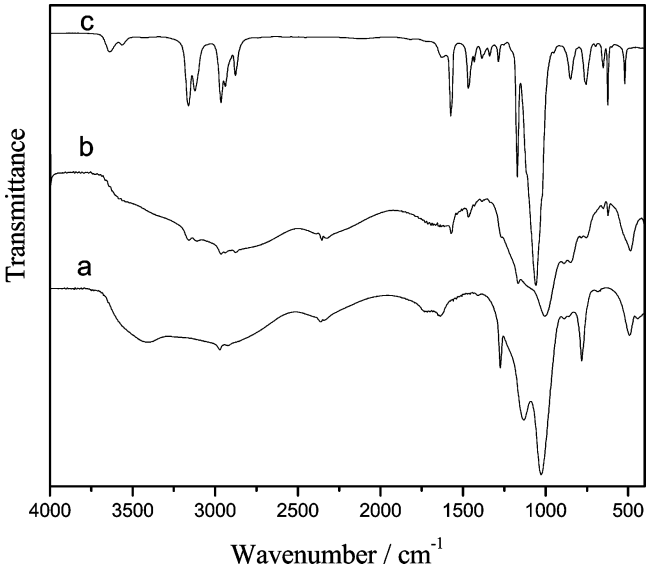

Figure 4. FTIR spectra of the electrolytes (a) without RTIL, (b) with RTIL, and (c) $BMImBF_4$.

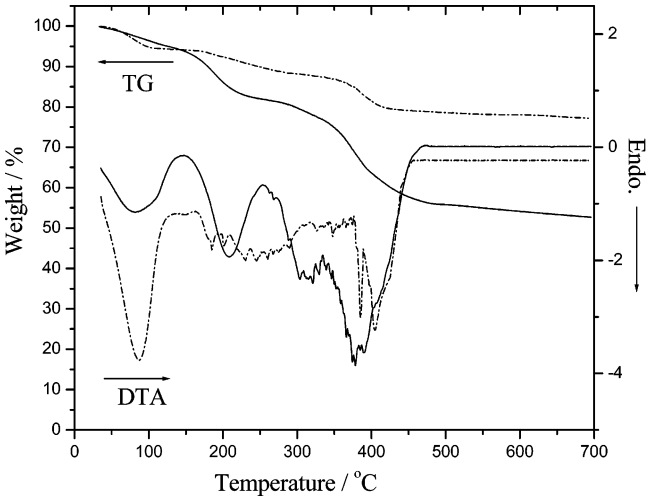

Figure 5. TG and DTA curves of the electrolytes without (broken line) and with (solid line) RTIL.

vibration of the $H_2PO_4^-$ groups, and the B−F stretching vibration of $BMImBF_4$.[37] Hence, it became hard to observe the changes of the ν(B−F) mode and the ν(O−P) mode when RTIL was incorporated into the MSQ matrix. However, the peak of the Si−O−Si vibration mode shifted from 1027 to 1005 cm^{-1} and became wider with the addition of the RTIL. One of the reasons might be that the structure-directing RTIL induced the growth of the long chains of the Si−O−Si, at the expense of the short Si−O−Si chains (1132 cm^{-1}). Furthermore, compared with the spectra of GE and neat RTIL,[37,38] the peaks of the ring stretch 1574 and 1468 cm^{-1} became wider, and the frequency of the P−O vibration mode shifted from 492 to 488 cm^{-1}, which could be attributed to the interaction of hydrogen-bonding between RTIL and H_3PO_4.[29] This was also proved by evidence from other spectrum measurement.

3.5. Thermal and Dynamic Mechanical Analysis. The TG and DTA curves are shown in Figure 5 for the electrolytes GE and IL-GE. The TG curve of GE showed a weight loss below 110 °C, which was caused by the evaporation of physically adsorbed free water, while further loss at the higher temperature was assigned to the evaporation of strongly adsorbed water in the gel electrolyte or the dehydration of phosphoric acid. For the IL-GE, the two-step evaporation process was likely to proceed, whereas the strongly adsorbed water was much more than the physically adsorbed water. As discussed above, because of the presence of hydrogen-bonding, a strong interaction between RTIL and water enhanced the retention of the adsorbed water, and the contained ingredients in IL-GE did not leach or desorb from the surface easily. The weight loss above 300 °C might be ascribed to the decomposition of the MSQ matrix and RTIL[39] since there were only endothermic peaks in the DTA curves. The resultant proton-conducting electrolytes, therefore, possess a good thermal stability up to 300 °C.

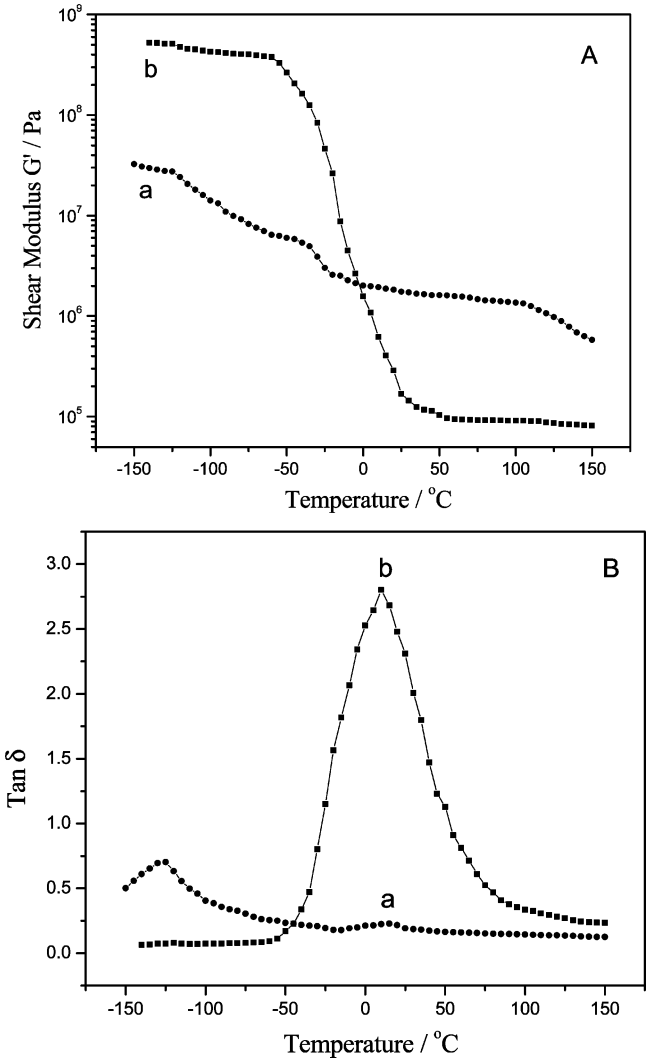

Figure 6. Temperature dependence of (A) shear modulus and (B) tan δ of the electrolytes (a) without and (b) with RTIL. Heating rate: 3 °C/min; frequency: 10 Hz.

The thermomechanical behavior of the electrolyte was evaluated by temperature dependence of the shear modulus and the loss factor tan δ shown in Figure 6.[40] At very low temperatures, the IL-GE showed a plateau in modulus at a magnitude of 5×10^8 Pa, which was that of a hard rubber material. As the temperature increased, the membrane exhibited a glass region showing an abrupt decrease of the modulus and finally reached another plateau about 8×10^4 Pa. The abrupt decrease in shear modulus and the peak of tan δ around 10 °C can be attributed to the glass transition of the MSQ chains. The GE without RTIL showed a smaller decrease in shear modulus and a broader peak of tan δ compared with the IL-GE. In evidence, the RTIL-templated electrolyte became more elastic than the conventional GE at ambient temperature. We ascribed this phenomenon to the high viscosity of the RTIL (219 cP,

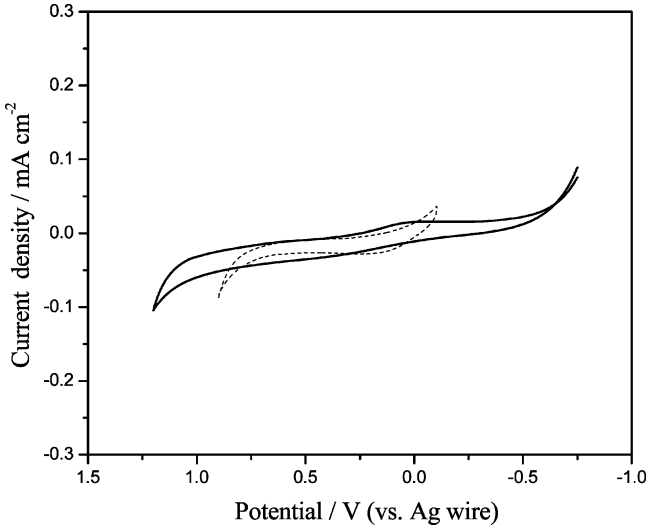

Figure 7. Cyclic voltammograms of the electrolytes without (broken line) and with (solid line) RTIL. Working and counter electrodes: stainless steels; reference electrode: Ag wire; scan rate: 10 mV/s.

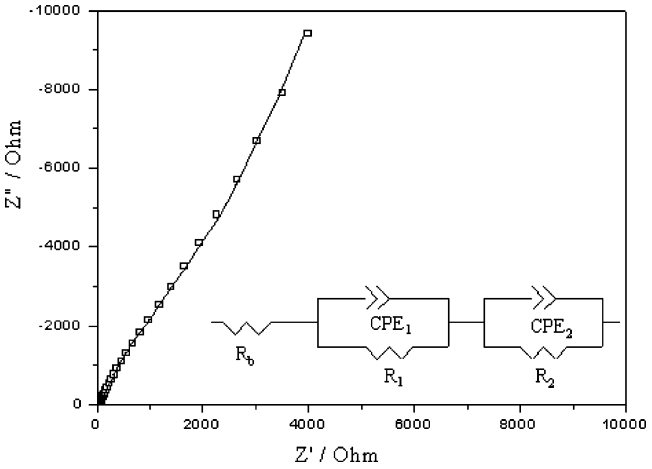

Figure 8. Typical complex impedance plot (squares) and the corresponding fitted curve (solid line) of the RTIL-templated electrolyte. Inset is the equivalent circuit mode of the impedance plot. Symbols Z′ and Z″ refer to the real and imaginary components; data were collected at open circuit with ac perturbation signal of 10 mV and the frequency range of 100 kHz to1 Hz. R_b, R_1, and R_2 stand for the bulk resistance, the SS electrode/electrolyte double-layer interface impedance, and the diffusive impedance of the migrating ions in the electrolyte, respectively; CPE_1 and CPE_2 correspond to the capacitances of the double layer and the bulk electrolyte, respectively.

298 K)[33] and the electrostatic interactions among the molecules of $BMImBF_4$ and the MSQ matrix.[41]

3.6. Electrochemical Properties. By means of the cyclic voltammetry technique, the electrochemical windows of IL-GE and GE were compared. The cyclic voltammetry curves of GE and IL-GE are presented in Figure 7. It was obvious that the RTIL-templated electrolyte had the wider electrochemical window (1.5 V) than that of GE (1.0 V). This phenomenon was mainly attributed to the good electrochemical stability of RTIL and the hydrogen-bonding between RTIL and water, the latter of which reduced the free water, as discussed in TG. Thus, the RTIL-templated electrolyte showed superior electrochemical properties.

The complex impedance plot for SS/electrolyte/SS sandwiched structure is shown in Figure 8. The spectrum shows an inconspicuous arc in the high-frequency range and a straight line in the low-frequency range. The disappearance of the

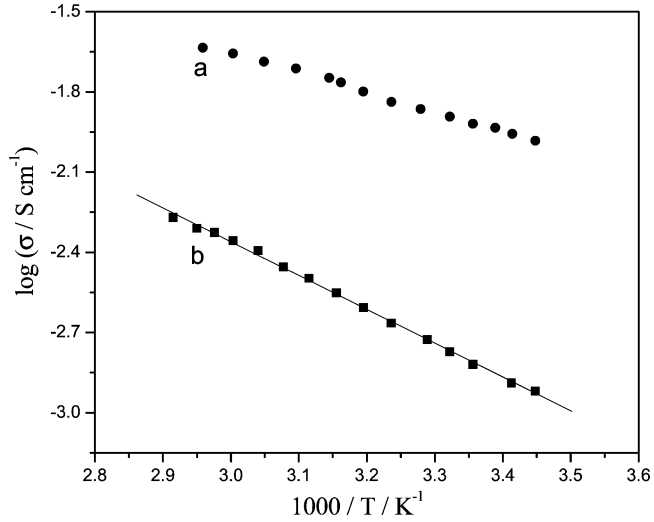

Figure 9. Temperature dependence of the ionic conductivities for the electrolytes (a) without and (b) with RTIL. Solid line was the Arrhenius equation fitted result for the RTIL-templated electrolyte.

semicircle in impedance spectra at high frequency is explained with a good contact between electrodes and electrolyte. The high-frequency arc represents the double-layer capacitance between electrolyte/electrode interface, while the straight line after the arc is due to the migration of ions and the surface in-homogeneity of the electrodes. As it could be seen from Figure 8, our experiment data were well fitted to the equivalent circuit

$$R_b(\mathrm{CPE}_1R_1)(\mathrm{CPE}_2R_2) \quad (1)$$

Here, R_b, (CPE_1R_1), and (CPE_2R_2) represent the bulk resistance, the SS electrode/electrolyte double-layer interface impedance, and the diffusive impedance of the migrating ions in the electrolyte, respectively. In general, a CPE element is used in the model in place of a capacitor to compensate for in-homogeneity in the system.[42] In the ZView software, the CPE is defined by two parameters, CPE-T and CPE-P. CPE-T indicates the value of capacitance of the CPE element, while CPE_1-P indicates the change of the compressed semicircle from an ideal semicircle and CPE_2-P is a parameter indicating the slope of the low-frequency straight line. Hence, CPE_1 corresponds to the double-layer capacity between electrolyte/electrode interfaces; CPE_2 represents the bulk electrolyte capacitance and the roughness of the electrodes used. The bulk electrolyte resistance R_b and CPE can be estimated from this fitting procedure and the ionic conductivity (σ) of the gel electrolyte is calculated by

$$\sigma = l/(AR_b) \quad (2)$$

where l is the thickness of the electrolyte and A is the area of the SS electrode.

The variations of ionic conductivities with the reciprocal of temperature for GE and IL-GE are shown in Figure 9. When the temperature increased from 17 to 70 °C, the conductivities of both the electrolytes increased. It can be seen that the conductivity of GE was higher than that of IL-GE. Room-temperature (17 °C) conductivity up to 9×10^{-3} S cm^{-1} has been achieved for GE and 1.2×10^{-3} S cm^{-1} for IL-GE. With the addition of RTIL, the conductivity was slightly decreased because of the high viscosity of RTIL, the dilution effect of RTIL, and the hydrogen-bonding between RTIL and H_3PO_4/water.

The relationship between log σ and 1000/T of the GE looked like a straight line in this temperature range (ca. 17−70 °C). Matsuda et al.[43] have already explained that the temperature dependence of conductivity of the H_3PO_4-doped silica gels followed the Vogel−Tamman−Fulcher (VTF) equation in the wide temperature range (−80 to 100 °C). Since the preparation method and the visual inspection of the GE in the present study was similar to ref 43, the temperature dependence of conductivity should not be Arrhenius-type but the VTF-type, and protons transferred through a liquidlike path in micropores of the H_3PO_4-doped MSQ macroscopic solid.

In IL-GE, the dependence between log σ and temperature can be fitted reasonably by Arrhenius equation but not by VTF equation in this temperature range, and the correlation coefficient (R^2) is ≥0.98. The activation energy for proton conduction was 24.7 kJ/mol, and the lower activation energy suggested the possibility of proton transport via a Grotthus type mechanism.[5] In the MSQ electrolyte, the solvent water can be easily protonated by H_3PO_4, and the proton conduction can occur via Grotthus type mechanism in which there is an exchange of protons between protonated and unprotonated water molecules with the possible participation of dissociated species such as $H_2PO_4^-$, HPO_4^{2-}, $H_4PO_4^+$, or undissociated H_3PO_4. The proton formed a H_3O^+ ion and jumped to the neighboring lone pair of electrons of a water molecule. These trends were seen in high-porosity silica xerogels also.[44] This type of conduction process has a low activation energy for conduction and relatively high ambient temperature ionic conductivities result. As discussed above, the hydrogen-bonding between RTIL and H_3PO_4 or water might exist in IL-GE. Because of the hydrogen-bonding and the high viscosity of $BMImBF_4$ (η = 219 cP, 298 K;[33] cf. H_2O, 0.89 cP; toluene, 0.59 cP), the strong interaction with the MSQ matrix influenced H_3PO_4 dissociation or the coordination sphere of the protons; probably, the protonic carriers such as H_3O^+ or $H_5O_2^+$ were bound in the matrix and the continuous pathways for protonic conduction were not straightway in the IL-GE. The hopping motion of ions was affected since the hopping motion involved hydrogen-bond forming and breaking process and the high viscosity of $BMImBF_4$ reduced the ionic diffusion coefficients and thus lowered the conductivity of IL-GE. A converse effect as temperature increased was due to the reduced viscosity and the separation of hydrogen-bonding aggregation.

Although the conductivity of IL-GE was slightly lower than that of GE, the IL-GE showed wider electrochemical windows and long-term stability on ionic conductivity as well as thermomechanical properties, which were the more important aspects in the practical application. On the other hand, proton-conducting electrolytes such as H_3PO_4-doped silica gel and Nafion are very sensitive to the variation of relative humidity (r. h.), while the IL-GE in our work can keep high conductivity at low r. h. and at temperatures in the low and medium range because of the retention of large amounts of strongly adsorbed water and show less dependence on humidity. Work along this line is in progress.

4. Conclusion

Proton-conducting electrolytes were synthesized by the sol−gel process of alkoxysilane in the presence of room-temperature ionic liquid. The addition of $BMImBF_4$ into the MTMOS precursor solution did not accelerate the sol−gel process, but the RTIL influenced the morphology of synthesized MSQ and manifested itself as a template for the MSQ generated in the system. XPS and FTIR spectra of the RTIL-templated electrolyte proved that the hydrogen-bonding between $BMImBF_4$ and H_3PO_4/water was formed, which supported the backbone of the MSQ. The gelatinous electrolytes with RTIL did not shrink and the dopant did not leach out during storage and thus showed long-term stability on ionic conductivity and thermomechanical properties. Because of the presence of RTIL, the stability window reached 1.5 V and the proton conductivity reached 1.2×10^{-3} S cm^{-1} at room temperature. The satisfactory thermomechanical and electrochemical properties of the obtained electrolytes make them promising materials in various electrochemical devices including batteries, fuel cells, sensors, and electrochromic windows.

Acknowledgment. This work was financially supported by the National Natural Science Foundation of China (No. 20125513), Li Foundation, USA, and A Foundation for the Author of National Excellent Doctoral Dissertation of PR China.

References and Notes

(1) Lassegues, J. C. In *Proton Conductors: Solids, Membranes and Gels-Materials and Devices*; Colomban, P., Ed.; Cambridge University Press: Cambridge, U.K., 1992; Chapter 20.
(2) Wieczorek, W.; Stevens, J. R. *Polymer* **1997**, *38*, 2057.
(3) Nakamura, O.; Kodama, T.; Ogino, I.; Miyake, Y. *Chem. Lett.* **1979**, 17.
(4) Hatakeyama, K.; Sakaguchi, H.; Ogawa, K.; Inoue, H.; Iwakura, C.; Esaka, T. *J. Power Sources* **2003**, *124*, 559.
(5) Raducha, D.; Wieczorek, W.; Florjanczyk, Z.; Stevens, J. R. *J. Phys. Chem.* **1996**, *100*, 20126.
(6) Zukowska, G.; Rogowska, M.; Weczkowska, E.; Wieczorek, W. *Solid State Ionics* **1999**, *119*, 289.
(7) Zukowska, G.; Chojnacka, N.; Wieczorek, W. *Chem. Mater.* **2000**, *12*, 3578.
(8) Antonucci, P. L.; Arico, A. S.; Creti, P.; Ramunni, E.; Antonucci, V. *Solid State Ionics* **1999**, *125*, 431.
(9) Sumner, J. J.; Creager, S. E.; Ma, J. J.; Desmarteau, D. D. *J. Electrochem. Soc.* **1998**, *145*, 107.
(10) Chandra, S.; Sekhon, S. S.; Srivastava, R.; Arora, N. *Solid State Ionics* **2002**, *154−155*, 609.
(11) Chandra, S.; Sekhon, S. S.; Srivastava, R.; Arora, N. *Solid State Ionics* **2002**, *152−153*, 741.
(12) Srivastava, R.; Chandra, S. *Phys. Status Solidi A* **2002**, *191*, 202.
(13) Matsuda, A.; Kanzaki, T.; Tadanaga, K.; Tatsumisago, M.; Minami, T. *Solid State Ionics* **2002**, *154−155*, 687.
(14) Matsuda, A.; Kanzaki, T.; Tadanaga, K.; Tatsumisago, M.; Minami, T. *Electrochim. Acta* **2001**, *47*, 939.
(15) Matsuda, A.; Kanzaki, T.; Kotani, Y.; Tatsumisago, M.; Minami, T. *Solid State Ionics* **2001**, *139*, 113.
(16) Seddon, K. R.; Stark, A.; Torres, M. J. *Pure Appl. Chem.* **2000**, *72*, 2275.
(17) Welton, T. *Chem. Rev.* **1999**, *99*, 2071.
(18) Ogihara, W.; Sun, J.; Forsyth, M.; MacFarlane, D. R.; Yoshizawa, M.; Ohno, H. *Electrochim. Acta* **2004**, *49*, 1797.
(19) Nakagawa, H.; Izuchi, S.; Kuwana, K.; Nukuda, T.; Aihara, Y. *J. Electrochem. Soc.* **2003**, *150*, 695.
(20) Doyle, M.; Choi, S. K.; Proulx, G. *J. Electrochem. Soc.* **2000**, *147*, 34.
(21) Susan, M. A. B. H.; Noda, A.; Mitsushima, S.; Watanabe, M. *Chem. Commun.* **2003**, 938.
(22) Lewandowski, A.; Swiderska, A. *Solid State Ionics* **2003**, *161*, 243.
(23) Ue, M.; Takeda, M.; Toriumi, A.; Kominato, A.; Hagiwara, R.; Ito, Y. *J. Electrochem. Soc.* **2003**, *150*, 499.
(24) Lewandowski, A.; Galinski, M. *J. Phys. Chem. Solids* **2004**, *65*, 281.
(25) Matsumoto, H.; Matsuda, T.; Tsuda, T.; Hagiwara, R.; Ito, Y.; Miyazaki, Y. *Chem. Lett.* **2001**, 26.
(26) Mikoshiba, S.; Murai, S.; Sumino, H.; Hayase, S. *Chem. Lett.* **2002**, 1156.
(27) Wang, P.; Zakeeruddin, S. M.; Comte, P.; Exnar, I.; Grätzel, M. *J. Am. Chem. Soc.* **2003**, *125*, 1166.
(28) Lu, W.; Fadeev, A. G.; Qi, B. H.; Smela, E.; Mattes, B. R.; Ding, J.; Spinks, G. M.; Mazurkiewics, J.; Zhou, D.; Wallace, G. G.; MacFarlane, D. R.; Forsyth, S. A.; Forsyth, M. *Science* **2002**, *297*, 983.
(29) Zhou, Y.; Schattka, J. H.; Antonietti, M. *Nano Lett.* **2004**, *4*, 477.
(30) Zhou, Y.; Antonietti, M. *Chem. Commun.* **2003**, 2564.
(31) Zhou, Y.; Antonietti, M. *Adv. Mater.* **2003**, *15*, 1452.
(32) Zhou, Y.; Antonietti, M. *Chem. Mater.* **2004**, *16*, 544.

(33) Huddleston, J. G.; Visser, A. E.; Reichert, W. M.; Willauer, H. D.; Broker, G. A.; Rogers, R. D. *Green Chem.* **2001**, *3*, 156.
(34) Shchipunov, Y. A.; Karpenko, T. Y. *Langmuir* **2004**, *20*, 3882.
(35) Leo, C. J.; Subba Rao, G. V.; Chowdari, B. V. R. *Solid State Ionics* **2002**, *148*, 159.
(36) Padovani, A. M.; Rhodes, L.; Allen, S. A. B.; Kohl, P. A. *J. Electrochem. Soc.* **2002**, *149*, 161.
(37) Koel, M. *Proc. Estonian Acad. Sci. Chem.* **2000**, *49*, 145.
(38) Tait, S.; Osteryoung, R. A. *Inorg. Chem.* **1984**, *23*, 4352.
(39) Sudhir, N. V. K. A.; Brennecke, J. F.; Samanta, A. *Chem. Commun.* **2001**, 413.
(40) Matejka, L.; Dukh, O.; Kamisova, H.; Hlavata, D.; Spirkova, M.; Brus, J. *Polymer* **2004**, *45*, 3267.
(41) Tsuruhara, K.; Hara, K.; Kawahara, M.; Rikukawa, M.; Sanui, K.; Ogata, N. *Electrochim. Acta* **2000**, *45*, 1223.
(42) Qian, X. M.; Gu, N. Y.; Cheng, Z. L.; Yang, X. R.; Wang, E. K.; Dong, S. J. *Electrochim. Acta* **2001**, *46*, 1829.
(43) Iwakura, C.; Kumagae, K.; Yoshiki, K.; Nohara, S.; Furukawa, N.; Inoue, H.; Minami, T.; Tatsumisago, M.; Matsuda, A. *Electrochim. Acta* **2003**, *48*, 1499.
(44) Colomer, M. T.; Anderson, M. A. *J. Non-Cryst. Solids* **2001**, *290*, 93.